arXiv:cond-mat/0107375v1 [cond-mat.str-el] 18 Jul 2001

Optical investigation on the electronic structures of $Y_2Ru_2O_7$, $CaRuO_3$, $SrRuO_3$, and $Bi_2Ru_2O_7$

J. S. Lee, Y. S. Lee, and T. W. Noh
School of Physics and Research Center for Oxide Electronics, Seoul National University, Seoul 151-747, Korea

K. Char, Jonghyurk Park, and S.-J. Oh
School of Physics and Center for Strongly Correlated Materials Research, Seoul National University, Seoul 151-747, Korea

J.-H. Park
Department of Physics and electron Spin Science Center, Pohang University of Science and Technology, Pohang 790-784, Korea

C. B. Eom
Department of Materials Science and Engineering, University of Wisconsin-Madison, Madison, WI 53706, USA

T. Takeda and R. Kanno
Department of Chemistry, Kobe University, Hyogo 657, Japan

(February 1, 2008)

Abstract

We investigated the electronic structures of the bandwidth-controlled ruthenates, $Y_2Ru_2O_7$, $CaRuO_3$, $SrRuO_3$, and $Bi_2Ru_2O_7$, by optical conductivity analysis in a wide energy region of 5 meV $\sim$ 12 eV. We could assign optical transitions from the systematic changes of the spectra and by comparison with the O 1*s* x-ray absorption data. We estimated some physical parameters, such as the on-site Coulomb repulsion energy and the crystal-field splitting energy. These parameters show that the 4*d* orbitals should be more extended than 3*d* ones. These results are also discussed in terms of the Mott-Hubbard model.

PACS number; 78.20.-e, 78.30.-j, 78.66.-w

Typeset using REVTEX

I. INTRODUCTION

The Mott transition has been widely studied in strongly correlated electron systems as one of the most important mechanisms for metal-insulator transition.[1] For $3d$ transition metal oxides, which have rather localized electron orbitals, the electron-electron (*el-el*) correlation becomes significant and plays important roles in determining their physical properties. Up to now, most works on the Mott transition have been focused on the $3d$ transition metal oxides, especially with early transition metals, such as Ti and V.[2] On the other hand, for $4d$ and $5d$ transition metal oxides, it has been known that the *el-el* correlation becomes weaker due to their more extended d orbitals.

Since unconventional superconductivity was observed for Sr_2RuO_4,[3] there has been large interest in ruthenates. Although ruthenates belong to the $4d$ transition metal oxides, some experimental works have suggested that the correlation effects play important roles. By investigating optical conductivity spectra $\sigma(\omega)$ of $SrRuO_3$, Kostic *et al.* claimed that its electrodynamics could not be explained by the Fermi-liquid theory.[4] Lee *et al.* reported observation of pseudogap formation in $BaRuO_3$, which has some similarities with the pseudogaps of high T_c superconductors.[5] From photoelectron spectroscopy (PES) and x-ray absorption (XAS) measurements of $SrRuO_3$, Fujioka *et al.* reported that its electron correlation effects should be considered to be important.[6]

Electrical properties of the ternary ruthenates show systematic changes from a Mott insulator to a band metal. $Y_2Ru_2O_7$ has the pyrochlore structure and shows an insulating behavior. Both $CaRuO_3$ and $SrRuO_3$ have the perovskite structures and show metallic responses. Note that $SrRuO_3$ is more metallic than $CaRuO_3$, and that $SrRuO_3$ becomes ferromagnetic below 160 K. $Bi_2Ru_2O_7$ has the pyrochlore structure and behaves as a Pauli paramagnetic metal. All of the above pyrochlore and perovskite ruthenates have four $4d$ electrons in the Ru 4+ ions with the low spin configuration. Since all of the ruthenates have three-dimensional networks of corner-shared RuO_6 octahedra, they are expected to have similar electronic structures. Cox *et al.* investigated systematically the electronic structures of the ruthenates using PES and electron energy loss spectroscopy.[7] Their results were consistent with a progressive decrease in the transfer-energy integral that determines the Ru $4d$ bandwidth in the series $Y_2Ru_2O_7$ <$CaRuO_3$ <$SrRuO_3$ <$Bi_2Ru_2O_7$, and the insulating behavior of $Y_2Ru_2O_7$ could be understood in terms of the correlation-induced electron localization, i.e. the Mott transition.

An optical spectroscopy measurement in a wide spectral region is also known to be a powerful tool to analyze the electronic structures of some highly correlated electron systems.[8] In this paper, we investigated the electronic structures of the ternary ruthenates, $Y_2Ru_2O_7$, $CaRuO_3$, $SrRuO_3$, and $Bi_2Ru_2O_7$ by measuring reflectivity spectra from 5 meV to 30 eV. Their $\sigma(\omega)$ showed systematic changes as the Ru $4d$ bandwidth increased. Combined with the O $1s$ XAS data, we could determine optical transitions of ruthenates. We found that the old assignments of the transitions by one of us (T.W.N.),[9] related to the Hubbard bands and the quasi-particle (QP) band of the perovskite ruthenates, were not correct. Such a mistake occurred because the assignments were made solely on the basis of $\sigma(\omega)$ below 5 eV. However, in this study, the transition assignments were made based on $\sigma(\omega)$ of four different compounds in a much wider spectral region. And, the assignments were also consistent with the O $1s$ XAS data. From the fitting on $\sigma(\omega)$ of $CaRuO_3$, we could estimate some physical

quantities, such as the on-site Coulomb repulsion energy U and the crystal field splitting $10Dq$.

II. EXPERIMENTAL TECHNIQUES

Optical spectra of the perovskite ruthenates were measured using epitaxial films. The $SrRuO_3$ and the $CaRuO_3$ films were epitaxially grown on the $SrTiO_3$ substrates using the pulsed laser deposition and sputtering techniques, respectively.[10,11] The film thicknesses were larger than 4000 Å, which are much thicker than the penetration depth of the light, so the reflected light from the $SrTiO_3$ substrates became negligible. For the $CaRuO_3$ films, it is well known that their transport properties can be changed significantly, namely from a metal to an insulator, by strain effects.[11] To obtain films whose properties were similar to those of a bulk sample, we used a substrate with a large miscut angle of $5 \sim 7$ °.

Optical spectra of the pyrochlore ruthenates were measured using high density polycrystalline samples. The $Bi_2Ru_2O_7$ and $Y_2Ru_2O_7$ polycrystalline samples were synthesized by sintering under a high pressure of around 3 GPa.[12] Such a high pressure was applied to obtain high density samples, since it was difficult to obtain reliable optical data using samples with high porosity. Since the pyrochlore phase is a cubic phase, the optical constants of the pyrochlore ruthenates should be isotropic. So, we could determine their optical constants even from polycrystalline samples. Before optical measurements, the surfaces of the polycrystalline samples were polished up to 0.3 μm. After optical measurements, thin gold films were evaporated on the samples and used to make corrections due to scattering from rough sample surfaces.

We measured reflectivity spectra from 5 meV to 30 eV using numerous spectrophotometers at room temperature. In the energy region between 5 meV and 0.6 eV, we used a conventional Fourier transform spectrophotometer. Between 0.5 eV and 6.0 eV, we measured the spectra using a grating spectrophotometer. In the deep ultraviolet region above 6.0 eV, we used the synchrotron radiation from the normal incidence monochromator beam line at Pohang Accelerator Laboratory. From the reflectivity spectra in a wide region, we used the Kramers-Kronig (K-K) transform to obtain $\sigma(\omega)$. For this analysis, the reflectivity below 5 meV was extrapolated with the Hagen-Rubens relation for the metallic ruthenate samples and with a constant value for the insulating $Y_2Ru_2O_7$ sample. For a high frequency region, the reflectivity value at 30 eV was used for reflectivities up to 40 eV, above which ω^{-4} dependence was assumed. We found that the results presented in this paper were nearly independent of the details of the extrapolation. To check the validity of our K-K analysis, we also independently determined $\sigma(\omega)$ using spectroscopic ellipsometry techniques in the photon energy range of $1.5 \sim 5.5$ eV. $\sigma(\omega)$ data from the spectroscopic ellipsometry agreed quite well with the results from the K-K analysis.[13]

III. RESULTS AND ANALYSIS

Figure 1 shows room temperature $\sigma(\omega)$ of $Y_2Ru_2O_7$, $CaRuO_3$, $SrRuO_3$, and $Bi_2Ru_2O_7$. As displayed in Figs. 1(a) and (b), the spectra of $Y_2Ru_2O_7$, $CaRuO_3$, and $SrRuO_3$ show similar interband transitions in the energy region between 3 and 12 eV. Three strong peaks

around 3, 6, and 10 eV are commonly observed. These facts indicate that the electronic structures of these compounds should be quite similar. However, $\sigma(\omega)$ of $Bi_2Ru_2O_7$ looks different from those of other ruthenates. While the peak around 10 eV disappears, the peak around 6 eV is much enhanced. [Nevertheless, as we will show later, these features also can be understood in terms of an electronic structure which is basically similar to those of other ruthenates, and the differences in the spectral distribution come from the differences in the allowed transitions.]

It should be noted that the spectra in the energy region below 2.5 eV vary from a sample to a sample. As shown in Fig. 1(a), $\sigma(\omega)$ of $Y_2Ru_2O_7$ does not have any Drude-like peak, in agreement with the fact that it is in an insulating state. Also, a rather weak peak appears around 1.7 eV. As shown in Fig. 1(b), $\sigma(\omega)$ of $CaRuO_3$ has a coherent Drude-like peak and an incoherent weak peak around 1.7 eV, which is quite similar to that observed in $Y_2Ru_2O_7$. On the other hand, $\sigma(\omega)$ of $SrRuO_3$ and $Bi_2Ru_2O_7$ have the Drude-like peaks, but do not show any peak around 1.7 eV. Since the ruthenates become more metallic as it goes from $Y_2Ru_2O_7$ to $Bi_2Ru_2O_7$, the systematic changes of the coherent Drude-like peak and the incoherent peak around 1.7 eV could be closely related to electrical properties of the systems.

Figure 2 is a schematic diagram for the electronic structure of $CaRuO_3$. The diagram is mainly composed of three parts: (1) the Ru $4d$ states near E_F, (2) the O $2p$ states around 5 eV below E_F, and (3) the unoccupied Ca $3d$ states around 6 eV above E_F. $CaRuO_3$ is a metallic compound very close to the Mott transition.[7] According to the dynamic mean field theory,[14] for a metallic sample near the Mott transition, its one particle spectral function will be split into two Hubbard bands in addition to the QP band located at E_F. Therefore, the Ru $4d$ states might be split into upper and lower Hubbard bands by the on-site Coulomb repulsion energy U with the QP band at E_F. And, the upper Hubbard band might be further splits into states of the t_{2g} and the e_g symmetries by $10Dq$.

To explain the electronic structures of other compounds, we should make two minor modifications in Fig. 2. First, the unoccupied Ca $3d$ states should be replaced by the unoccupied Y $4d$, Sr $4d$, or Bi $6p$ states. For the Y $4d$ and Bi $6p$ states, they might be located at energies lower than those of the Ca $3d$ and Sr $4d$ states and could overlap with the e_g states.[15,16] Second, the details of the Ru $4d$ states near E_F should vary according to the *el-el* correlation effect. For insulating $Y_2Ru_2O_7$, the Hubbard bands are completely split due to the large *el-el* correlation, and the QP peak disappears.[7] On the other hand, for a band metal, such as $Bi_2Ru_2O_7$, the *el-el* correlation becomes quite weak, and the Hubbard bands merge to form a single partially filled band at E_F. For $SrRuO_3$, the structures of the Ru $4d$ states might be close to those for $Bi_2Ru_2O_7$, because $SrRuO_3$ is known to be less correlated than $CaRuO_3$.[7] [Note that, with such changes, the diagram in Fig. 2 becomes consistent with the results of the PES and the XAS experiments on $SrRuO_3$[15] and $(Bi,Y)_2Ru_2O_7$.[16]]

To understand $\sigma(\omega)$ of $CaRuO_3$, we considered all of the possible optical transitions, which were marked as solid lines at the top of the electronic structure diagram in Fig. 2. According to the Fermi's golden rule,[17] the optical transition rate from an initial state $|i\rangle$ to a final state $|f\rangle$ can be written as

$$I_{i\to f} \sim |\langle f|\vec{r}_o \cdot \vec{p}|i\rangle|^2 \rho_i \rho_f, \tag{1}$$

where ρ_i and ρ_f are densities of states for $|i\rangle$ and $|f\rangle$, respectively. Inside the transition

matrix element, $\vec{r}_o$ is the space unit operator, and $\vec{p}$ is the momentum operator. For an isolated atom, the transition matrix element allows electric dipole transitions with the selection rule of $\Delta L = \pm 1$, where ΔL means the difference between the angular momentum quantum numbers for the state $|i\rangle$ and $|f\rangle$. For solids, the matrix element also depends on the overlap integral between $|i\rangle$ and $|f\rangle$ states. Since the O $2p$ bands are hybridized with the Ru $4d$ and the Ca $3d$ bands, the transitions from the O $2p$ to the Ru t_{2g} (Transition A), the Ru e_g (Transition B), and the Ca $3d$ states (Transition C) will be allowed. The transitions between the Ru $4d$ states should be forbidden in an isolated atom. However, in real oxides, some interatomic transitions could be allowed, and some intraatomic transition might be possible due to the hybridization with the O $2p$ bands and/or local distortions.[8] [Note that the transitions between the Ru $4d$ states should be much weaker than the charge transfer transitions from the O $2p$ to the Ru $4d$ states.] For $CaRuO_3$, three transitions from the occupied Ru t_{2g} states to the unoccupied Ru t_{2g} (Transition α), the Ru e_g (Transition β) and the Ca $3d$ states (Transition γ) were considered. [Other transitions involving the QP states were possible, but found to be quite small except for the Drude peaks for metallic samples.]

Interestingly, most of the expected interband transitions are observed in $\sigma(\omega)$ of $CaRuO_3$. As shown in Fig. 3, $\sigma(\omega)$ of $CaRuO_3$ is composed of three strong peaks around 3, 6, and 10 eV, and two weak peaks around 1.7 and 4.3 eV. The large differences in peak strengths might be originated from the different characters of each excitation. We fitted $\sigma(\omega)$ of $CaRuO_3$ below 12 eV with a Drude model and five Lorentz oscillators, whose contributions are represented by the dotted lines.[18] The functional forms of the Lorentz oscillators are

$$\sigma(\omega) = \sum_i \frac{S_i \Gamma_i \omega_i^2}{(\omega^2 - \omega_i^2)^2 + \Gamma_i^2 \omega_i^2}, \tag{2}$$

where S_i, Γ_i, and ω_i represent the strength, the damping constant, and the frequency of the ith Lorentz oscillator, respectively. The values of the fitting parameters are listed in TABLE I. Note that the oscillator strengths of i=2, 4, and 5 are stronger by about a factor of 5 than those of i=1 and 3.

To assign the interband transitions of $CaRuO_3$ properly, we found that it was very helpful to check $\sigma(\omega)$ of $Y_2Ru_2O_7$. As shown in Fig. 1(a), the first and the second peaks appear at 1.7 eV and 3.2 eV, respectively, which are similar to the low lying peak positions of $CaRuO_3$. Considering that $Y_2Ru_2O_7$ is a Mott insulator, we assigned the lowest peak as the transition between the Hubbard bands. Actually, similar features were also observed in other insulating ruthenates, such as Ca_2RuO_4 and c-axis Sr_2RuO_4.[19,20] Thus, it is quite reasonable that the oscillators of i=1 and 2 for $CaRuO_3$ should be assigned as Transitions α and A, respectively. Considering the energy differences between each excitation and their relative strengths, we assigned the oscillators of i=4 and 5 as Transitions B and C, respectively. Our fitting also shows that there is another weak oscillator around 4.36 eV, which was assigned as Transition β. Note that this transition should have much lower strength than any other transitions due to the selection rule, and that this excitation could not be seen in $\sigma(\omega)$ of other ruthenates.

Our peak assignments of $CaRuO_3$ are also consistent with the results of the O $1s$ XAS experiments, which probe the unoccupied states of the Ru $4d$ and the Ca $3d$ orbitals which are strongly hybridized with the O $2p$ orbitals. As shown in the inset of Fig. 3, three peaks were observed around 530, 533, and 537 eV. The near edge intensities around 530 and 533

eV are attributed to the states with the mixed O 2p-Ru 4d characters of the t_{2g} and the e_g states, respectively. And, the peak around 537 eV comes from the Ca 3d states. The peak positions of the Ru e_g and the Ca 3d states relative to the unoccupied Ru t_{2g} states are about 3 and 7 eV, respectively. These energy differences are consistent with those between the optical p-d transitions A and B (3.14 eV), and A and C (6.47 eV), respectively. This indicates that our peak assignments are quite reasonable.

Based on the assignments for $\sigma(\omega)$ of $CaRuO_3$, $\sigma(\omega)$ of the other ruthenates can be assigned in similar ways. For $Y_2Ru_2O_7$, the distinct peaks near 3 and 6 eV can be assigned as Transitions A and B, respectively. And, the peak around 9 eV can be assigned as Transition C from the O 2p states to the Y 4d states. For $SrRuO_3$, Transitions A and B can be assigned in a similar way, and Transition C from the O 2p states to the Sr 4d states appears around 10 eV. On the other hand, these peak values of the p-d transitions are smaller by about 3.0 eV than the energy difference between the corresponding states whose positions were measured by PES and XAS.[15] The difference might be due to the formation of an exciton in the optical process, whose binding energy will lower the value of transition peak. Also, the spectral weights lying closer to E_F would contribute to $\sigma(\omega)$ more significantly than those further away from E_F, so the measured value of transition energy in $\sigma(\omega)$ could be smaller than the actual energy separation of the initial and final states.

As shown in Fig. 1, $\sigma(\omega)$ of $Bi_2Ru_2O_7$ is quite different from the other spectra. However, we can still explain its optical spectra using an electronic structure similar to those of other ruthenates. For $Bi_2Ru_2O_7$, the unoccupied Bi 6p states, instead of the d states for other ruthenates, are located very close to the e_g states.[16] While Transition B is expected near 6 eV, Transition C between the O 2p and the Bi 6p states should be quite weak due to the selection rule. On the other hand, Transition γ from the Ru t_{2g} to the Bi 6p states becomes possible, and should be located at lower energy than Transition C. Thus, the strong 6 eV structure for $Bi_2Ru_2O_7$ can be attributed to Transitions B and γ, which are located at similar energies.[21]

Up to this point, for some Mott-Hubbard systems, there have been controversies about assignments of the interband transitions related to Hubbard bands. For example, in $(Sr,Ca)VO_3$, the assignment of the U peak, i.e. transition between the Hubbard bands, was the subject of controversy, but was settled recently.[22,23] In ruthenates also, assignments for 1.7 and 3.0 eV transitions have been controversial.[9,24] Ahn *et al.* assigned the 3.0 eV peak as Transition α,[9] but Dodge *et al.* attributed the peak as a charge transfer transition from the O 2p to the Ru t_{2g} states.[24] Based on $\sigma(\omega)$ studies in a much wider photon energy region and the XAS studies, we finally concluded that peaks around 1.7 and 3.0 eV should be assigned as Transitions α and A, respectively.

IV. DISCUSSION

From our optical analysis, we can obtain some important physical parameters such as U and $10Dq$. The photon energy of the d-d transition, i.e. Transition α, corresponds to the value of U. [Note that the U obtained from $\sigma(\omega)$ will be smaller than the energy difference between the upper and the lower Hubbard bands whose positions are determined by the PES and XAS due to the exciton and the screening effects.] Our study shows that the U values of $Y_2Ru_2O_7$ and $CaRuO_3$ are quite similar, i.e. about 1.7 eV. And, the energy difference

between Transitions A and B corresponds to $10Dq$. For all of the ruthenates we studied, the $10Dq$ values are around 3.0 eV, which is consistent with the theoretical results.[25,26]

It would be quite useful to compare the U and $10Dq$ values of the ruthenates with those of other $3d$ transition metal oxides, which were obtained from optical measurements. The values of U, i.e. about 1.7 eV, in ruthenates are much smaller than those in the $3d$ transition metal oxides which have similar numbers of d electrons. For example, in case of manganites with three or four electrons per Mn ion, the value of U was estimated to be larger than 3 eV.[8] Instead, the value of U for $CaRuO_3$ is very similar to that of vanadates which have two electrons per V ion.[23,27] The small value of U in ruthenates might be due to the fact that $4d$ electrons have more extended wavefunctions than $3d$ electrons. And, the value of $10Dq$ around 3 eV in ruthenates is larger than that of the $3d$ transition metal oxides, such as 2.3 eV for Ni-oxides,[28] 1.1 $\sim$ 1.8 eV for Mn-oxides.[29,30] The anisotropic Coulomb potential due to the surrounding oxygen ions could influence the $4d$ orbitals more strongly due to its larger size. Both the small value of U and the large value of $10Dq$ in ruthenates indicate that the $4d$ orbitals should be more extended than $3d$ ones.

It was found that the general behaviors of our spectra could be well explained in the regime of the Mott-Hubbard model with the bandwidth control. As the bandwidth increases, the system becomes more metallic, and the spectral weight of the Hubbard bands transfers to the QP peak at E_F. Accordingly, the d-d transitions related to the Hubbard bands, such as Transitions α and β, are expected to become weaker. As it goes from $Y_2Ru_2O_7$ to $Bi_2Ru_2O_7$, the distinct Transition α in $Y_2Ru_2O_7$ becomes weaker and finally disappears in $SrRuO_3$ and $Bi_2Ru_2O_7$. Especially for $CaRuO_3$, its $\sigma(\omega)$ shows the coherent peak as well as Transition α, which could be a typical optical feature of a correlated metal near the Mott transition.[27] Simultaneously, Transition A shifts to a lower energy by about 0.6 eV, which might be related to the merging of the t_{2g} bands to E_F which were originally split due to the correlation effects. These results are quite consistent with Cox *et al.*'s photoemission work, which suggested that ruthenates should belong to the class of bandwidth-controlled Mott-Hubbard systems.[7]

V. SUMMARY

We investigated optical properties of $Y_2Ru_2O_7$, $CaRuO_3$, $SrRuO_3$, and $Bi_2Ru_2O_7$ in a wide energy region from 5 meV to 12 eV. Their optical conductivity spectra obtained through the Kramers-Kronig transformation show the systematic variation from a Mott insulator of $Y_2Ru_2O_7$ to a band metal of $Bi_2Ru_2O_7$. The general behaviors of the optical spectra could be well explained by the Mott-Hubbard model. Combined with O $1s$ x-ray absorption measurements, the optical excitations were properly assigned based on the electronic structures. From the peak assignments, we could estimate some physical parameters, such as the on-site Coulomb repulsion energy and the crystal field splitting energy. Compared to such parameters of the $3d$ transition metal oxides, the results could describe the more extended character of the $4d$ orbitals in ruthenates.

ACKNOWLEDGMENTS

We would like to thank Jaejun Yu, Yunkyu Bang, and J. Okamoto for useful discussions. This work was supported by the Ministry of Science and Technology through the Creative Research Initiative program, and by KOSEF through the Center for Strongly Correlated Materials Research. The work at POSTECH was supported by POSTECH research funds. The experiments at PLS were supported by MOST and POSCO.

REFERENCES

[1] N. F. Mott, *Metal-insulator transitions* (Taylor & Francis Ltd., London, 1974).

[2] M. Imada, A. Fujimori, and Y. Tokura, Rev. Mod. Phys. **70**, 1039 (1998) and references therein.

[3] Y. Maeno, H. Hashimoto, K. Yoshida, S. Nishizaki, T. Fujita, J. G. Bednorz, and F. Lichtenberg, Nature **372**, 532 (1995).

[4] P. Kostic, Y. Okada, N. C. Collins, Z. Schlesinger, J. W. Reiner, L. Klein, A. Kapitulnik, T. H. Geballe, and M. R. Beasley, Phys. Rev. Lett. **81**, 2498 (1998).

[5] Y. S. Lee, J. S. Lee, K. W. Kim, T. W. Noh, Jaejun Yu, E. J. Choi, G. Cao, and J. E. Crow, accepted in Europhys. Lett..

[6] K. Fujioka, J. Okamoto, T. Mizokawa, A. Fujimori, I. Hase, M. Abbate, H. J. Lin, C. T. Chen, Y. Takeda, and M. Takano, Phys. Rev. B **56**, 6380 (1997).

[7] P. A. Cox, R. G. Egdell, J. B. Goodenough, A. Hamnett, and C. C. Naish, J. Phys. C: Solid State Phys. **16**, 6211 (1983).

[8] J. H. Jung, K. H. Kim, D. J. Eom, T. W. Noh, E. J. Choi, J. Yu, Y. S. Kwon, and Y. Chung, Phys. Rev. B **55**, 15489 (1997).

[9] J. S. Ahn, J. Bak, H. S. Choi, T. W. Noh, J. E. Han, Y. Bang, J. H. Cho, and Q. X. Jia, Phys. Rev. Lett. **82**, 5321 (1999).

[10] L. Mieville, T. H. Geballe, L. Antognazza, and K. Char, Appl. Phys. Lett. **70**, 126 (1997).

[11] R. A. Rao, Q. Gan, R. J. Cava, Y. Suzuki, S. C. Gausepohl, Mark Lee, C. B. Eom, Appl. Phys. Lett. **70**, 3035 (1997).

[12] T. Takeda, M. Nagata, H. Kobayaxhi, R. Kanno, Y. Kawamoto, M. Takano, T. Kamiyama, F. Izumi, and A. W. Sleight, J. Solid State Chem. **140**, 182 (1998).

[13] H. J. Lee, J. H. Jung, Y. S. Lee, J. S. Ahn, T. W. Noh, K. H. Kim, and S.-W. Cheong, Phys. Rev. B. **60**, 5251 (1999).

[14] A. Georges, G. Kotliar, W. Krauth, and M. J. Rezenberg, Rev. Mod. Phys. **68**, 13 (1996) and references therein.

[15] J. Okamoto, T. Mizokawa, and A. Fujimori, Phys. Rev. B **60**, 2281 (1999).

[16] Jonghyurk Park, S.-J. Oh, J.-H. Park, and K. H. Kim, to be published.

[17] F. Wooten, *Optical Properties of Solids* (Academic press, New York and Londen, 1972).

[18] Actually, the coherent part in $CaRuO_3$ cannot be fitted with the simple Drude model. This feature has many similarities with the case of $SrRuO_3$. [See Ref. 4.] Since the coherent contribution and Transition α are well separated in $\sigma(\omega)$ of $CaRuO_3$, the fitting for the coherent part with simple Drude model does not influence significantly the determination of Transition α.

[19] V. Puchkov, M. C. Schabel, D. N. Basov, T. Startseva, G. Cao, T. Timusk, and Z.-X. Shen, Phys. Rev. Lett. **81**, 2747 (1998).

[20] T. Katsufuji, M. Kasai, and Y. Tokura, Phys. Rev. Lett. **76**, 126 (1996).

[21] XAS data of $Bi_2Ru_2O_7$, in Ref. 16, show that the density of the e_g states becomes large, which could also make the oscillator strength of Transition B strong.

[22] H. Makino, I. H. Inoue, M. J. Rozenberg, I. Hase, Y. Aiura, and S. Onari, Phys. Rev. B **58**, 4384 (1998).

[23] H. F. Pen, M. Abbate, A. Fujimori, Y. Tokura, H. Eisaki, S. Uchida, and G. A. Sawatzky, Phys. Rev. B **59**, 7422 (1999).

[24] J. S. Dodge, E. Kulatov, L. Klein, C. H. Ahn, J. W. Reiner, L. Mieville, T. H. Geballe,

M. R. Beasley, A. Kapitulnik, H. Ohta, Yu. Uspenskii, and S. Halilov, Phys. Rev. B **60**, R6987 (1999).

[25] D. Singh, J. Appl. Phys. **79**, 4818 (1996).

[26] The experimental and theoretical studies on $SrRuO_3$ reported that the exchange energy is around 0.5 and 0.65 eV, respectively. [Refer to Ref. 8 and 25.] The comparably large $10Dq$ and the small exchange energy guarantee that the electrons in the Ru ion show the low spin configuration.

[27] M. J. Rozenberg, G. Kotliar, H. Kajueter, G. A. Thomas, D. H. Rapkine, J. M. Honig, and P. Metcalf, Phys. Rev. Lett. **75**, 105 (1995).

[28] T. Higuchi, T. Tsukamoto, M. Watanabe, M. M. Grush, T. A. Gallcott, R. C. Perera, D. L. Ederer, Y. Tokura, Y. Harada, Y. Tezuka, and S. Shin, Phys. Rev. B **60**, 7711 (1999).

[29] Y. Moritomo, T. Arima, and Y. Tokura, J. Phys. Soc. J. **64**, 4117 (1995).

[30] K. Takenaka, Y. Sawaki, R. Shiozaki, and S. Sugai, Phys. Rev. B **62**, 13864 (2000).

[31] The metallic state of $Bi_2Ru_2O_7$ has not been well understood yet. Actually, its coherent peak in $\sigma(\omega)$ is very broad, compared to those of the other metallic systems. As one possible explanation, Cox *et al.* argued that the hybridization in the Bi-O-Ru network is so strong that it could make the Ru $4d$ bandwidth large enough for the system to be metallic.[See Ref. 7.]

FIGURES

FIG. 1. Room temperature optical conductivity spectra $\sigma(\omega)$ of (a) $Y_2Ru_2O_7$, (b) $CaRuO_3$ and $SrRuO_3$, and (c) $Bi_2Ru_2O_7$. The indecies of each peak indicate the corresponding optical excitations, which are displayed in Fig. 2.

FIG. 2. A schematic diagram of the electronic structures of $CaRuO_3$. Near E_F, the occupied and unoccupied Ru t_{2g} states are located with the QP states at E_F. There are the e_g states above the unoccupied t_{2g} states. Outside these Ru d states, there are the occupied O $2p$ states and the unoccupied Ca $3d$ states. Other ruthenates, namely, $Y_2Ru_2O_7$, $SrRuO_3$, and $Bi_2Ru_2O_7$, should have similar electronic structures with a couple of differences, which are described in the text.

FIG. 3. Detailed analysis on $\sigma(\omega)$ of $CaRuO_3$. The fitted results (a solid line) are well consistent with the experimental data of $\sigma(\omega)$ (solid circles). The contribution of the Drude term and five Lorentz oscillators are represented by the dotted lines. The Lorentz oscillator at 4.36 eV is shown as a thick dotted line for the eye. The dashed line indicates the background contribution from higher energy peaks above 12 eV which are not shown in this figure. The inset shows the experimental result of the O $1s$ x-ray absorption spectroscopy on $CaRuO_3$.

TABLES

TABLE I. Values of Lorentz oscillator fitting parameters for $CaRuO_3$.

	ω_i (eV)	Γ_i(eV)	S_i (Ω^{-1}cm$^{-1}\cdot$ eV)	Assignments
i=1 (Transition α)	1.71	1.30	658	$t_{2g} \rightarrow t_{2g}$
i=2 (Transition A)	3.08	1.82	2500	O $2p \rightarrow t_{2g}$
i=3 (Transition β)	4.36	1.57	661	$t_{2g} \rightarrow e_g$
i=4 (Transition B)	6.22	3.22	3950	O $2p \rightarrow e_g$
i=5 (Transition C)	10.55	2.20	2114	O $2p \rightarrow$ Ca $3d$

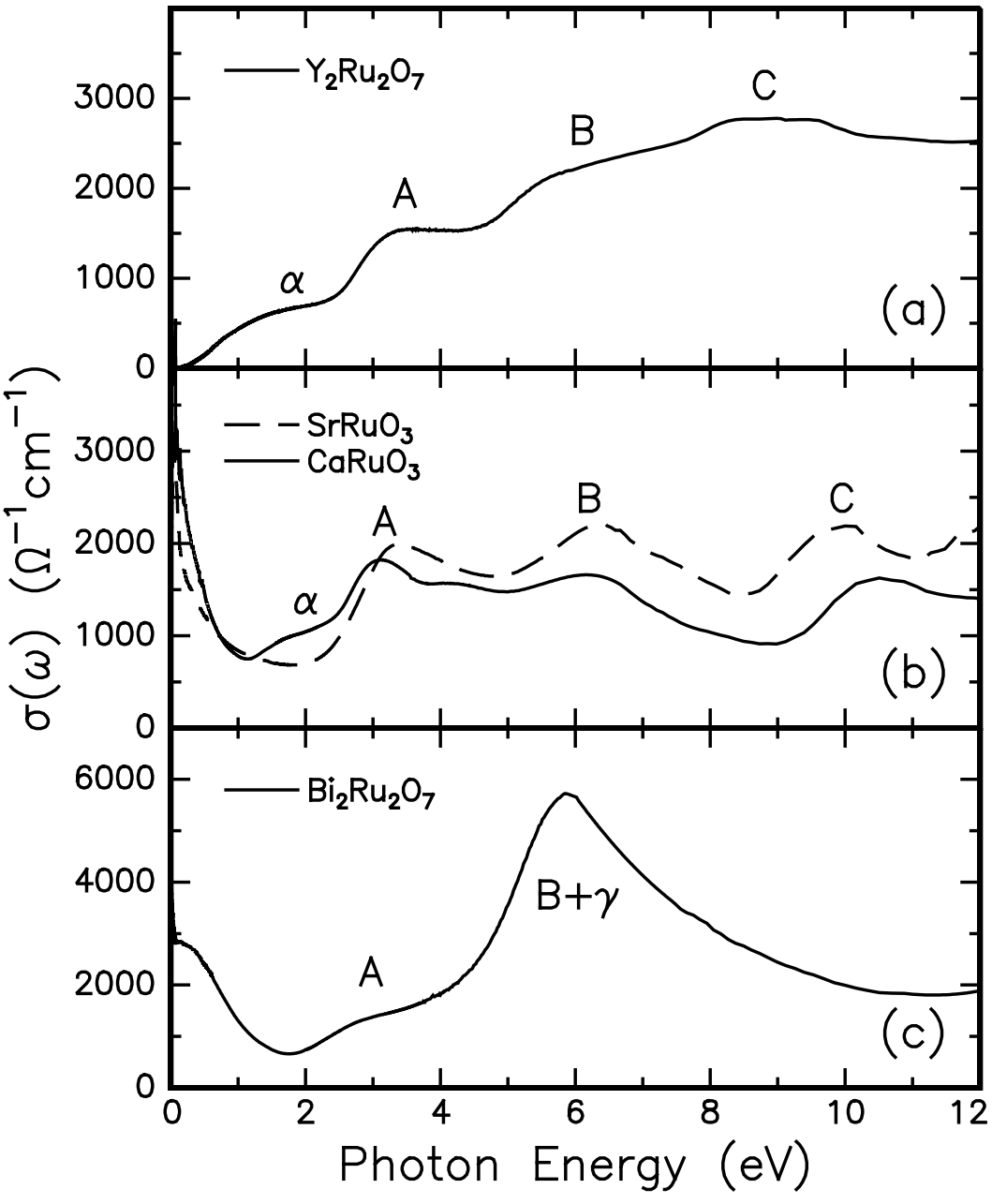
Y2Ru2O7
SrRuO3
CaRuO3
Bi2Ru2O7
α
A
B
C
B+γ
(a)
(b)
(c)
σ(ω) (Ω−1cm−1)
Photon Energy (eV)
0
1000
2000
3000
4000
6000
2
4
6
8
10
12

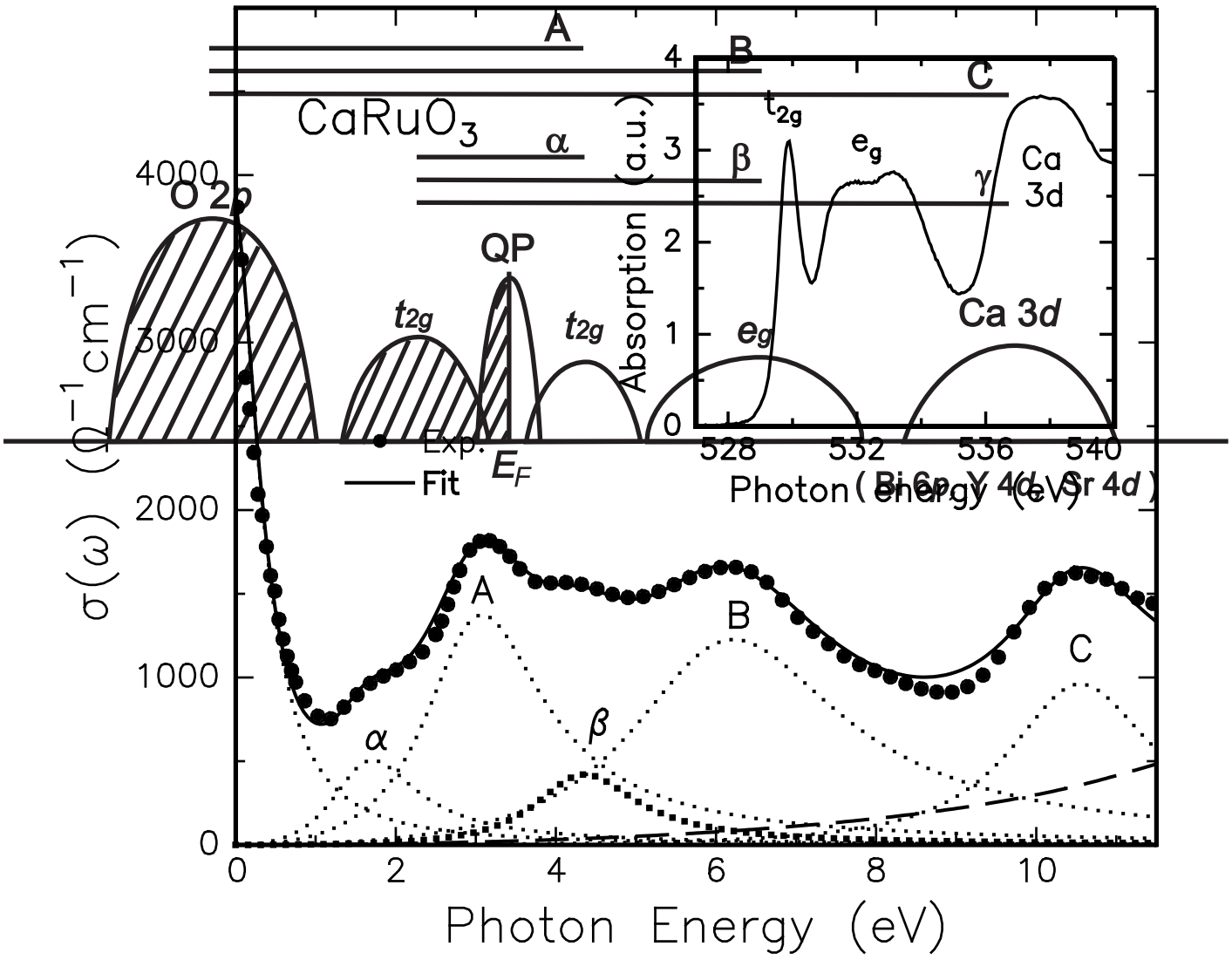
A
B
C
CaRuO3
α
O 2p
QP
t2g
t2g
Exp.
Fit
EF
σ(ω) (Ω−1cm−1)
Photon Energy (eV)
Absorption (a.u.)
t2g
eg
β
γ
Ca 3d
eg
Ca 3d
Photon energy (eV)
(Bi 6p, Y 4d, Sr 4d)
A
B
C
α
β
0
1000
2000
3000
4000
0
2
4
6
8
10
528
532
536
540
0
1
2
3
4